3

Induced Transmembrane Voltage—Theory, Modeling, and Experiments

Tadej Kotnik

Gorazd Pucihar

3.1 The Cell and the Induced Transmembrane Voltage

From the electrical point of view, the cell can roughly be described as an electrolyte (the cytoplasm) surrounded by an electrically insulating shell (the plasma membrane). Physiologically, the surroundings of the cell also resemble an electrolyte quite closely. Under such conditions, when a cell is exposed to an external electric field, the electric field in its very vicinity concentrates within the membrane, which thus shields the cytoplasm from the exposure (this is the reason why the internal structure of the cell is not too important, except for very short pulses and very high field frequencies discussed in Section 3.2.4). The concentration of the electric field inside the membrane results in an electric potential difference across it, termed the induced transmembrane voltage, which superimposes onto the resting transmembrane voltage typically present under physiological conditions. As the electric field vanishes, so does the induced component of transmembrane voltage. This voltage affects the functioning of voltage-gated membrane channels, initiates the action potentials, stimulates cardiac cells, and when sufficiently large, it can also lead to cell membrane electroporation (Bedlack et al. 1994, Cheng et al. 1999, Neumann et al. 1999, Teissié et al. 1999, Burnett et al. 2003, Sharma and Tung 2004, Huang et al. 2006).

With rapidly time-varying electric fields, such as waves with frequencies in the megahertz range or higher, or electric pulses with durations in the submicrosecond range, both the membrane and its surroundings have to be treated as materials with both a nonzero electric conductivity and a nonzero dielectric permittivity.

From the geometrical point of view, the cell can be characterized as a geometric body (the cytoplasm) surrounded by a shell of uniform thickness (the membrane). For a suspended cell, the simplest model is a sphere surrounded by a spherical shell. For augmented generality, the sphere can be replaced by a spheroid (or an ellipsoid), but in this case, the requirement of uniform thickness complicates the description of the shell substantially. If its inner surface is a spheroid or an ellipsoid, its outer surface lacks a simple geometrical characterization, and vice versa. Still, in the steady state, this does not affect the induced transmembrane voltage, which can still be determined analytically.

Spheres, spheroids, and ellipsoids may be reasonable models for suspended cells, but not for cells in tissues. No simple geometrical body can model a typical cell in a tissue, and furthermore every cell generally differs in its shape from the rest. With irregular geometries and/or with cells close to each other, the induced voltage cannot be determined analytically, and thus cannot be formulated as an explicit function. This deprives us of some of the insight available from explicit expressions, but using modern computers and numerical methods, the voltage induced on each particular irregular cell can still be determined quite accurately.

An alternative to both analytical and numerical determination of the induced transmembrane voltage is the experimental approach, which can be performed invasively using microelectrodes, or noninvasively by loading the cells with a potentiometric dye and measuring its fluorescence.

In Sections 3.2 through 3.4 we focus separately on the analytical derivation of the induced transmembrane voltage for the cells with simple shapes, numerical computation for the cells for which the analytical approach fails, and noninvasive experimental determination by means of potentiometric dyes.

3.2 Analytical Derivation

In this section, we present the course of derivation of the transmembrane voltage induced on a spherical cell placed into a homogeneous electric field. The reasons for including a detailed derivation, and not only a sketch of the essential steps, are the frequent requests (from both researchers and students) for a handout containing such a derivation, and the lack of readily available sources containing such a derivation (which might also explain these requests). Readers who are not interested in the technical details can skip to the final result, which is given by Equation 3.18, and continue reading from that point on.

3.2.1 Laplace's Equation

Transmembrane voltage is defined as the difference between the values of the electric potential on both sides of the membrane. The derivation of the induced component of this voltage is based on solving the equation

$$\nabla\left(\left(\sigma+\varepsilon\frac{\partial}{\partial t}\right)\nabla\Psi(x,y,z,t)\right)=0 \tag{3.1}$$

which describes the spatial and temporal distribution of the electric potential. For the steady-state situation, in which the time derivatives are zero, Equation 3.1 simplifies into the well-known Laplace's equation

$$\nabla\cdot\nabla\Psi(x,y,z)=0 \tag{3.2}$$

Solving this equation in a particular coordinate system gives the mathematical solution for the steady-state spatial distribution of Ψ in systems of objects that can be described in such a coordinate system. The mathematical solution is typically a rather large set of functions containing a number of arbitrary constants. By applying physically realistic boundary conditions, the number of functions in this set is

reduced, and the values of the constants are determined, yielding the physical solution that describes the actual spatial distribution of Ψ in the given system. The induced transmembrane voltage is then calculated as the difference between the electric potentials on both sides of the membrane.

In the following section, we illustrate this principle by solving Laplace's equation in spherical coordinates, thereby obtaining the description of Ψ in and around a spherical cell.

3.2.2 Spherical Cells

Although biological cells are not perfect spheres, in theoretical treatments they are often considered as such: a spherical interior (the cytoplasm) surrounded by a concentric spherical shell of uniform thickness (the membrane). For certain types of cells, and particularly for cells in suspensions, this is also a reasonable approximation.

To determine the spatial distribution of the electric potential in and around a spherical cell placed into a homogeneous electric field, we write Laplace's equation in the spherical coordinate system (Figure 3.1):

$$\nabla \cdot \nabla \Psi(r,\theta,\varphi) = \frac{1}{r^2}\left(\frac{\partial}{\partial r}\left(r^2 \frac{\partial \Psi(r,\theta,\varphi)}{\partial r}\right) + \frac{1}{\sin\theta}\frac{\partial}{\partial \theta}\left(\sin\theta \frac{\partial \Psi(r,\theta,\varphi)}{\partial \theta}\right) + \frac{1}{\sin^2\theta}\frac{\partial^2 \Psi(r,\theta,\varphi)}{\partial \varphi^2}\right) = 0 \tag{3.3}$$

We align the center of the cell with the origin of the system and orient its coordinates so that the direction of the external field is parallel to the coordinate line traced by r for $\theta = 0°$, $\varphi = 0°$, as shown in Figure 3.1. This yields a symmetry with respect to φ, in the sense that any coordinate circle traced by φ for (r = constant, θ = constant) is everywhere perpendicular to the field, and consequently $\partial\Psi/\partial\varphi = 0$.

Thus, for the treated case, we have $\Psi(r, \theta, \varphi) = \Psi(r, \theta)$, and Equation 3.3 simplifies into

$$\begin{aligned} &\frac{1}{r^2}\left(\frac{\partial}{\partial r}\left(r^2 \frac{\partial \Psi(r,\theta)}{\partial r}\right) + \frac{1}{\sin\theta}\frac{\partial}{\partial \theta}\left(\sin\theta \frac{\partial \Psi(r,\theta)}{\partial \theta}\right)\right) \\ &= \frac{\partial^2 \Psi(r,\theta)}{\partial r^2} + \frac{2}{r}\frac{\partial \Psi(r,\theta)}{\partial r} + \frac{1}{r^2}\frac{\partial^2 \Psi(r,\theta)}{\partial \theta^2} + \frac{\mathrm{ctg}\,\theta}{r^2}\frac{\partial \Psi(r,\theta)}{\partial \theta} = 0 \end{aligned} \tag{3.4}$$

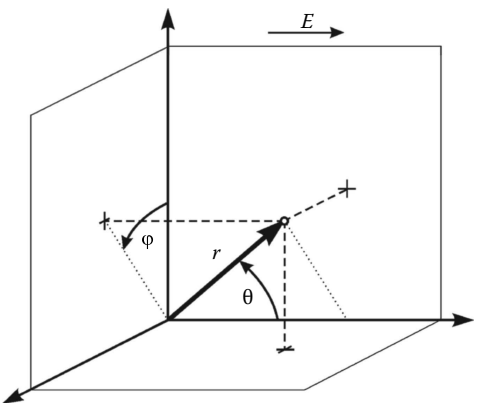

FIGURE 3.1 The spherical coordinate system and the orientation of the external field with respect to this system as used here in solving Laplace's equation for a spherical cell. The center of the cell is aligned with the origin of the system.

where we have applied the chain rule for derivatives. We now perform the separation of variables: we write the function Ψ as a product of two functions of a single variable

$$\Psi(r,\theta) = G(r)H(\theta) \tag{3.5}$$

and insert this form into Equation 3.4, obtaining

$$H(\theta)\left(\frac{\partial^2 G(r)}{\partial r^2} + \frac{2}{r}\frac{\partial(G(r))}{\partial r}\right) + \frac{G(r)}{r^2}\left(\frac{\partial^2 H(\theta)}{\partial \theta^2} + \operatorname{ctg}\theta\frac{\partial H(\theta)}{\partial \theta}\right) = 0 \tag{3.6}$$

Dividing both sides by $G(r)H(\theta)/r^2$, writing $\partial G/\partial r = G'(r)$, $\partial H/\partial\theta = H'(\theta)$, and transferring the functions of θ to the right-hand side of the equation, we get

$$\frac{r^2 G''(r) + 2rG'(r)}{G(r)} = -\frac{H''(\theta) + \operatorname{ctg}(\theta)H'(\theta)}{H(\theta)} \tag{3.7}$$

The left-hand side contains only functions of r, and is thus independent of the value of θ. Similarly, the right-hand side contains only functions of θ, and is thus independent of the value of r. Since according to Equation 3.7 the two sides are equal, it follows that they are independent of both r and θ, and must thus be equal to a certain constant. Denoting this constant by K, we thus get a system of two ordinary differential equations of second order

$$\begin{cases} r^2 G''(r) + 2rG'(r) - KG(r) = 0 \\ H''(\theta) + \operatorname{ctg}(\theta)H'(\theta) + KH(\theta) = 0 \end{cases} \tag{3.8}$$

The general solution of the first equation in Equation 3.8 is

$$G(r) = \begin{cases} C_1 r^{-1/2}\sin\left(\sqrt{-\frac{1}{4} - K}\log r\right) + C_2 r^{-1/2}\cos\left(\sqrt{-\frac{1}{4} - K}\log r\right), & K < -\frac{1}{4} \\ \frac{C_1}{r} + C_2, & K = -\frac{1}{4} \\ C_1 r^{-1/2\left(1-\sqrt{1+4K}\right)} + C_2 r^{-1/2\left(1+\sqrt{1+4K}\right)}, & K > -\frac{1}{4} \end{cases} \tag{3.9}$$

where C_1 and C_2 are arbitrary constants.

We now apply the first physically realistic boundary condition: as the distance from the cell increases, the distortion of the field by the cell decreases, and the electric field asymptotically approaches homogeneity, i.e., the state in which $\Psi(r, 0)$ is directly proportional to r. Since $H(\theta)$ is not a function of r, this implies that $G(r)$ is directly proportional to r, and in Equation 3.9 this only occurs for $K = 2$, where

$$G(r) = C_1 r + \frac{C_2}{r^2} \tag{3.10}$$

Since the value of K is the same in both differential equations in Equation 3.8, we can insert $K = 2$ into the second equation and solve it in this more specific form, obtaining

$$H(\theta) = C_3 \cos\theta + C_4 \left(1 - \cos\theta \log \sqrt{\frac{1+\cos\theta}{1-\cos\theta}} \right) \tag{3.11}$$

where C_3 and C_4 are arbitrary constants.

Accounting for the physically realistic boundary condition that $\Psi(r, \theta)$ is finite for all finite r and θ, it follows that $C_4 = 0$, since the term inside the parentheses in Equation 3.11 has singularities at $\theta = 0°$ and $\theta = 180°$. Therefore,

$$H(\theta) = C_3 \cos\theta \tag{3.12}$$

Joining Equation 3.10 and Equation 3.12 according to Equation 3.5, we get

$$\Psi(r,\theta) = \left(Ar + \frac{B}{r^2} \right) \cos\theta \tag{3.13a}$$

where A and B are arbitrary constants. This is the general physical solution for $\Psi(r, \theta)$ in a system consisting of a sphere, an arbitrary number of concentric spherical shells surrounding it, and the (infinite) space surrounding them, provided that the sphere and its shells are the only objects distorting the homogeneity of the electric field.

To come from the general physical solution to the specific one, in which also the constants A and B are determined, and thus the electric potential is fully described, we must now account for the particular geometrical and electrical properties of the system under our consideration. Our system consists of three regions: the cell interior (cytoplasm), the cell membrane, and the exterior, which differ in these properties, and hence also the values of A and B are in general different for each of these regions. Thus, we write

$$\Psi(r,\theta) = \begin{cases} \Psi_{\mathrm{i}}(r,\theta) = \left(A_{\mathrm{i}} r + B_{\mathrm{i}} r^{-2} \right) \cos\theta, & 0 \le r \le (R-d) \\ \Psi_{\mathrm{m}}(r,\theta) = \left(A_{\mathrm{m}} r + B_{\mathrm{m}} r^{-2} \right) \cos\theta, & (R-d) \le r \le R \\ \Psi_{\mathrm{e}}(r,\theta) = \left(A_{\mathrm{e}} r + B_{\mathrm{e}} r^{-2} \right) \cos\theta, & r \ge R \end{cases} \tag{3.13b}$$

where R is the cell radius and d is the membrane thickness.

We now proceed with applying the boundary conditions to determine the six constants in (Equation 3.13b). Since the actual Ψ is finite at $r = 0$, it follows that $B_{\mathrm{i}} = 0$. Requiring once again the field homogeneity far from the cell, this time writing explicitly the electric potential in a homogeneous field E,

$$\Psi(r, \theta) = -Er \cos\theta \tag{3.14}$$

we see that $A_{\mathrm{e}} = -E$.

The remaining four constants are determined by applying the continuity of the electric potential and the electric current density at the two interfaces between the regions.

$$\Psi_{\mathrm{i}}(R-d,\theta) = \Psi_{\mathrm{m}}(R-d,\theta) \tag{3.15a}$$

$$\Psi_m(R,\theta) = \Psi_e(R,\theta) \tag{3.15b}$$

$$\sigma_i \left.\frac{\partial \Psi_i(r,\theta)}{\partial r}\right|_{r=R-d} = \sigma_m \left.\frac{\partial \Psi_m(r,\theta)}{\partial r}\right|_{r=R-d} \tag{3.15c}$$

$$\sigma_m \left.\frac{\partial \Psi_m(r,\theta)}{\partial r}\right|_{r=R} = \sigma_e \left.\frac{\partial \Psi_e(r,\theta)}{\partial r}\right|_{r=R} \tag{3.15d}$$

where σ_i, σ_m, and σ_e denote the electric conductivities of the cytoplasm, the membrane, and the exterior, respectively. Inserting the explicit forms of Ψ_i, Ψ_m, and Ψ_e as given by (Equation 3.13b) into (Equations 3.15a through d), applying the already determined values $B_i = 0$ and $A_e = -E$, and treating the three conductivities as known constants, we obtain a system of four equations with four unknown constants (A_i, A_m, B_m, and B_e). Upon solving this system, we get

$$A_i = \frac{-9ER^3\sigma_e\sigma_m}{2R^3(\sigma_m+2\sigma_e)\left(\sigma_m+\frac{1}{2}\sigma_i\right)-2(R-d)^3(\sigma_e-\sigma_m)(\sigma_i-\sigma_m)} \tag{3.16a}$$

$$A_m = \frac{-3ER^3\sigma_e(\sigma_i+2\sigma_m)}{2R^3(\sigma_m+2\sigma_e)\left(\sigma_m+\frac{1}{2}\sigma_i\right)-2(R-d)^3(\sigma_e-\sigma_m)(\sigma_i-\sigma_m)} \tag{3.16b}$$

$$B_m = \frac{3ER^3(R-d)^3\sigma_e(\sigma_i-\sigma_m)}{2R^3(\sigma_m+2\sigma_e)\left(\sigma_m+\frac{1}{2}\sigma_i\right)-2(R-d)^3(\sigma_e-\sigma_m)(\sigma_i-\sigma_m)} \tag{3.16c}$$

$$B_e = \frac{ER^3\left[R^3(\sigma_m-\sigma_e)(2\sigma_m+\sigma_i)-(R-d)^3(\sigma_m-\sigma_i)(2\sigma_m+\sigma_e)\right]}{2R^3(\sigma_m+2\sigma_e)\left(\sigma_m+\frac{1}{2}\sigma_i\right)-2(R-d)^3(\sigma_e-\sigma_m)(\sigma_i-\sigma_m)} \tag{3.16d}$$

Inserting the expressions for A_m and B_m into Ψ_m as given by (Equation 3.13b), the induced transmembrane voltage can now be expressed as

$$\Delta\Psi_m = \Psi_m(R-d,\theta) - \Psi_m(R,\theta) = f_S ER\cos\theta \tag{3.17a}$$

where

$$f_S = \frac{3\sigma_e\left[3dR^2\sigma_i+(3d^2R-d^3)(\sigma_m-\sigma_i)\right]}{2R^3(\sigma_m+2\sigma_e)\left(\sigma_m+\frac{1}{2}\sigma_i\right)-2(R-d)^3(\sigma_e-\sigma_m)(\sigma_i-\sigma_m)} \tag{3.17b}$$

By applying a simplifying assumption that the membrane is a pure insulator, $\sigma_m = 0$, the function f_S turns into a constant, $f_S = 3/2$, and we obtain the well-known formula often referred to as the (steady-state) Schwan's equation:

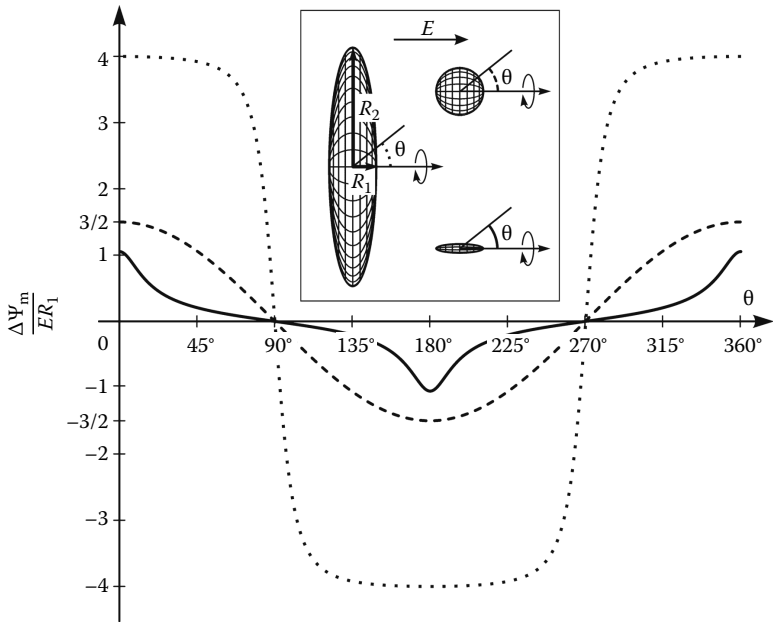

FIGURE 3.2 Normalized steady-state $\Delta\Psi_m$ as a function of the polar angle θ for spheroidal cells with the axis of rotational symmetry (ARS) aligned with the direction of the field. Solid: a prolate spheroidal cell with $R_2 = 0.2 \times R_1$. Dashed: a spherical cell, $R_2 = R_1 = R$. Dotted: an oblate spheroidal cell with $R_2 = 5 \times R_1$.

$$\Delta\Psi_m = \frac{3}{2} ER\cos\theta \tag{3.18}$$

This formula tells that the induced transmembrane voltage is proportional to the applied electric field and to the cell radius. Furthermore, it has extremal values at the points where the field is perpendicular to the membrane, i.e., at θ = 0° and θ = 180° (the "poles" of the cell), and in-between these poles it varies proportionally to the cosine of θ (see Figure 3.2, dashed).

Equation 3.18 describes the steady-state situation, which is typically established several microseconds after the onset of the electric field. With exposures to a DC field lasting hundreds of microseconds or more, this formula can safely be applied to yield the maximal, steady-state value of the induced transmembrane voltage. To describe the transient behavior during the initial microseconds, in addition to the electric conductivities one also has to account for the dielectric permittivity of the membrane, ε_m. Such a derivation, which is a slight extension of the derivation presented above (Pauly and Schwan 1959), yields the first-order Schwan's equation that reads

$$\Delta\Psi_m = \frac{3}{2} ER\cos\theta\left(1 - e^{-t/\tau_m}\right) \tag{3.19a}$$

where τ_m is the time constant of the membrane charging,

$$\tau_m = \frac{R\varepsilon_m}{2d\left(\sigma_i\sigma_e/(\sigma_i + 2\sigma_e)\right) + R\sigma_m} \tag{3.19b}$$

In certain experiments *in vitro*, where artificial extracellular media with conductivities substantially lower than physiological are used, the factor 3/2 is an oversimplification, and the more precise form given by Equation 3.17 must be used, as discussed in detail in Kotnik et al. (1997). But generally, the formulae

Equation 3.18 and Equation 3.19 are applicable to exposures to sine (AC) electric fields with frequencies below 1 MHz, and to rectangular electric pulses longer than 1 μs.

To determine the voltage induced by even higher field frequencies or even shorter pulses, the dielectric permittivities of the electrolytes also have to be accounted for. This leads to a further generalization of Equation 3.17 and/or Equation 3.19 to a second-order model (Grosse and Schwan 1992, Kotnik et al. 1998, Kotnik and Miklavčič 2000a), and the results it yields will be outlined in Section 3.2.4.

3.2.3 Spheroidal, Ellipsoidal, and Cylindrical Cells

Another direction of generalization is to assume a cell shape more general than that of a sphere. The most straightforward generalization is to a spheroid (a geometrical body obtained by rotating an ellipse around one of its radii, so that one of its orthogonal projections is a sphere, and the other two are the same ellipse) and further to an ellipsoid (a geometrical body in which each of its three orthogonal projections is a different ellipse). To obtain the analogues of Schwan's equation for such cells, one solves Laplace's equation in spheroidal and ellipsoidal coordinates, performing the same steps as in the solution in spherical coordinates described in detail in Section 3.2.2. A detailed description of the derivation in prolate and oblate spheroidal coordinates is given in Kotnik and Miklavčič (2000b), Gimsa and Wachner (2001), and Valič et al. (2003), and in analogy to Equation 3.18, for an oblate spheroid with the ARS aligned with the field it yields

$$\Delta\Psi_m = E\frac{R_2^2 - R_1^2}{\dfrac{R_2^2}{\sqrt{R_2^2 - R_1^2}}\operatorname{arcctg}\dfrac{R_1}{\sqrt{R_2^2 - R_1^2}} - R_1}\frac{R_2\cos\theta}{\sqrt{R_1^2\sin^2\theta + R_2^2\cos^2\theta}} \tag{3.20}$$

and for a prolate spheroid with the ARS aligned with the field

$$\Delta\Psi_m = E\frac{R_1^2 - R_2^2}{R_1 - \dfrac{R_2^2}{\sqrt{R_1^2 - R_2^2}}\ln\dfrac{R_1 + \sqrt{R_1^2 - R_2^2}}{R_2}}\frac{R_2\cos\theta}{\sqrt{R_1^2\sin^2\theta + R_2^2\cos^2\theta}} \tag{3.21}$$

where R_1 and R_2 are the radii of the spheroid in the directions parallel and perpendicular to the field, respectively (see also Figure 3.2).

Besides the fact that the expressions obtained for Ψ are somewhat more intricate than the one in spherical coordinates, the generalization of the shape from spherical to spheroidal invokes two additional complications outlined in the next two paragraphs.

A description of a cell is geometrically realistic if the thickness of its membrane is uniform. This is the case if the membrane represents the space between two concentric spheres, but not two confocal spheroids or ellipsoids. As a result, the thickness of the membrane modeled in spheroidal or ellipsoidal coordinates is necessarily nonuniform. By solving Laplace's equation in these coordinates, we thus obtain the spatial distribution of the electric potential in a nonrealistic setting. However, under the assumption that the membrane conductivity is zero, the induced transmembrane voltage obtained in this manner is still realistic. Namely, the shielding of the cytoplasm is then complete, and hence the electric potential everywhere inside the cytoplasm is constant. Therefore, the geometry of the inner surface of the membrane does not affect the potential distribution outside the cell, which is the same as if the cell would be a homogeneous nonconductive body of the same shape. A more rigorous discussion of the validity of this approach can be found in Kotnik and Miklavčič (2000b). Figure 3.2 compares the transmembrane voltage induced on two spheroids with the ARS aligned with the direction of the field, and that induced on a sphere.

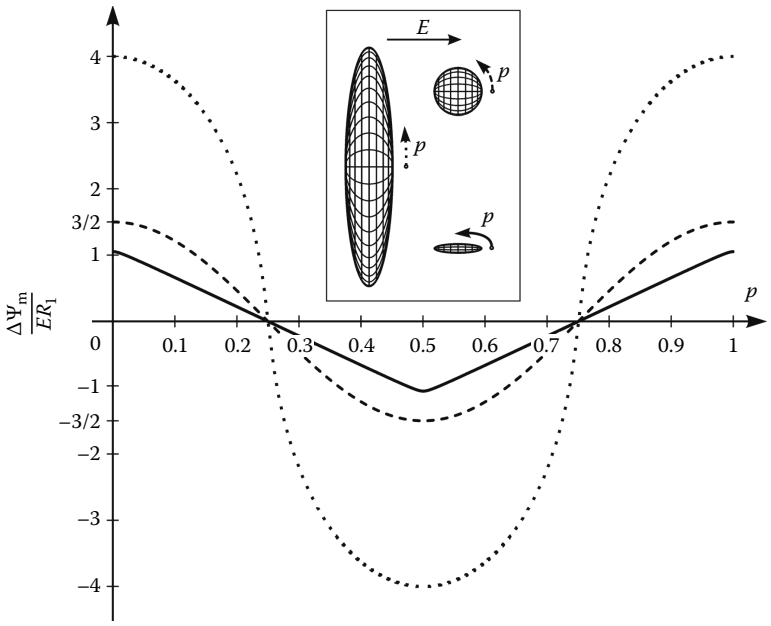

FIGURE 3.3 Normalized steady-state $\Delta\Psi_m$ as a function of the normalized arc length p for spheroidal cells with the ARS aligned with the direction of the field. Solid: a prolate spheroidal cell with $R_2 = 0.2 \times R_1$. Dashed: a spherical cell, $R_2 = R_1 = R$. Dotted: an oblate spheroidal cell with $R_2 = 5 \times R_1$.

For nonspherical cells, it is generally more revealing to express $\Delta\Psi_m$ as a function of the arc length than as a function of the angle θ (for a sphere, the two quantities are directly proportional). For uniformity, the normalized version of the arc length is used, denoted by p and increasing from 0 to 1 equidistantly along the arc of the membrane. This is illustrated in Figure 3.3 for the cells for which $\Delta\Psi_m(\theta)$ is shown in Figure 3.2, and all the plots of $\Delta\Psi_m$ henceforth will be presented in this manner.

Typically, $\theta(p)$ cannot be expressed by an elementary function, and $\Delta\Psi_m(p)$ has to be determined by numerical mapping. In analytical treatment of $\Delta\Psi_m$ in regular cell shapes for which such a treatment is possible, this mapping can be performed to arbitrary accuracy, but the process is somewhat tedious. In contrast, when $\Delta\Psi_m$ is computed numerically (see Section 3.3), the accuracy is limited by the size of the mesh employed, but the arc length is readily determined by the software, and the plots of $\Delta\Psi_m(p)$ are easy to generate.

Another complication caused by generalizing the cell shape from a sphere to a spheroid or an ellipsoid is that the induced voltage now also becomes dependent on the orientation of the cell with respect to the electric field. To deal with this, one decomposes the field vector into the components parallel to the axes of the spheroid or the ellipsoid, and writes the induced voltage as a corresponding linear combination of the voltages induced for each of the three coaxial orientations (Gimsa and Wachner 2001, Valič et al. 2003). Figures 3.4 and 3.5 show the effect of rotation of two different spheroids with respect to the direction of the field.

An analytical solution for $\Delta\Psi_m$ is also attainable for circular cylinders with the axis oriented perpendicularly to the external field, and is given by

$$\Delta\Psi_m = 2ER\cos\theta \tag{3.22}$$

This is a suitable approximation for elongated cellular structures such as muscle cells and axons of nerve cells, provided that the field is roughly perpendicular to their direction.

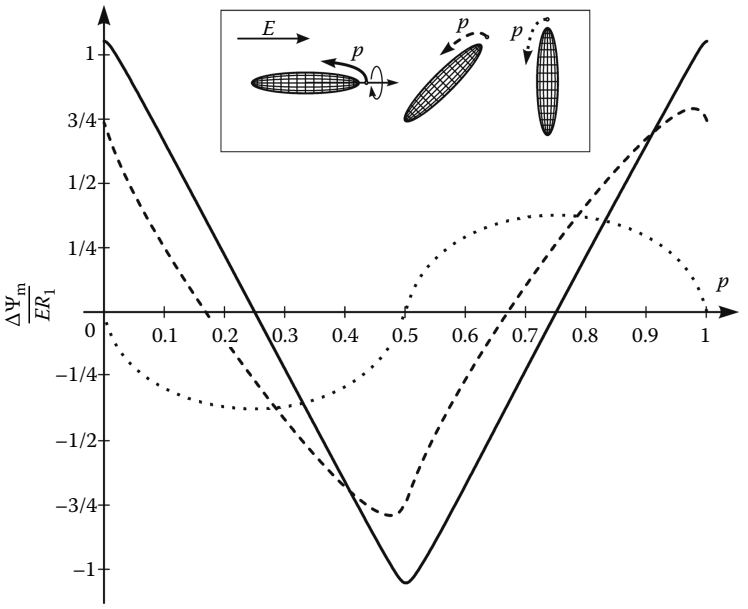

FIGURE 3.4 Normalized steady-state $\Delta\Psi_m(p)$ for a prolate spheroidal cell with $R_2 = 0.2 \times R_1$. Solid: ARS aligned with the field. Dashed: ARS at 45° with respect to the field. Dotted: ARS perpendicular to the field.

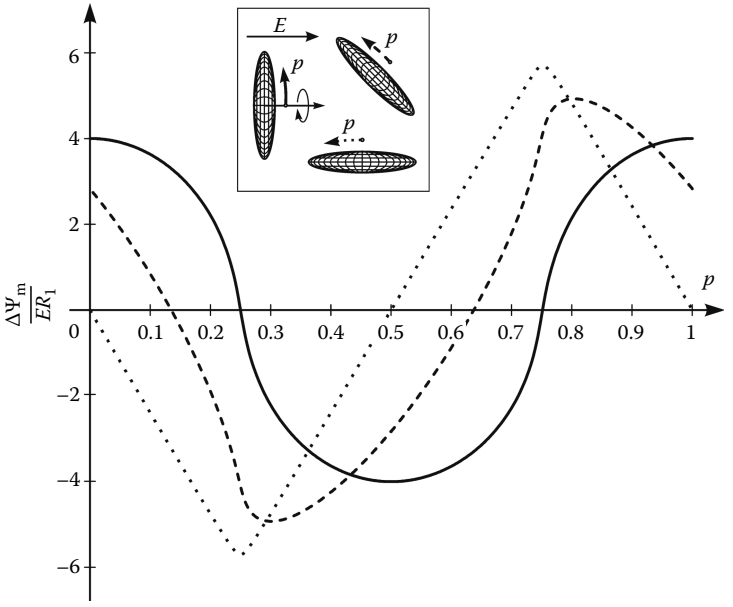

FIGURE 3.5 Normalized steady-state $\Delta\Psi_m(p)$ for an oblate spheroidal cell with $R_2 = 5 \times R_1$. Solid: ARS aligned with the field. Dashed: ARS at 45° with respect to the field. Dotted: ARS perpendicular to the field.

3.2.4 High Frequencies and Very Short Pulses

The time constant of the membrane charging (τ_m) given by (Equation 3.19b) implies that there is a delay between the time courses of the external field and the voltage induced by this field. As mentioned above, τ_m (and thus the delay) is somewhat below a microsecond under physiological conditions, but can be larger when cells are suspended in a low-conductivity medium. For alternating (AC) fields with the oscillation period much longer than τ_m, as well as with rectangular pulses much longer than τ_m, the amplitude of the induced voltage is very close to the steady-state value given by Equation 3.18. However, for AC fields with the period comparable or shorter than τ_m, as well as for rectangular pulses shorter than τ_m, the amplitude of the induced voltage starts to decrease.

To illustrate how the amplitude of the induced transmembrane voltage gets attenuated as the frequency of the AC field increases, we plot the normalized amplitude of the induced voltage as a function of the field frequency. For a spherical cell, the plot obtained is shown in Figure 3.6. The low-frequency plateau and the downward slope that follows are both described by the first-order Schwan's equation, but the high-frequency plateau is only described by the second-order model (Grosse and Schwan 1992, Kotnik et al. 1998, Kotnik and Miklavčič 2000a), in which all electric conductivities and dielectric permittivities have nonzero values.

With field frequencies approaching the GHz range, or with pulse durations in the nanosecond range, the attenuation of the voltage induced on the cell plasma membrane becomes so pronounced that this voltage becomes comparable to the voltage induced on organelle membranes in the cell interior. In certain circumstances, particularly if the organelle interior is electrically more conductive than the cytosol, or if the organelle membrane has a lower dielectric permittivity than the cell membrane, the voltage induced on the membrane of this organelle can temporarily even exceed the voltage induced on the plasma membrane (Kotnik and Miklavčič 2006). In principle, this could provide a theoretical explanation for a number of recent reports that very short and intense electric pulses (tens of ns, millions or tens of millions of V/m) can also induce electroporation of organelle membranes (Schoenbach et al. 2001, Beebe et al. 2003, Tekle et al. 2005).

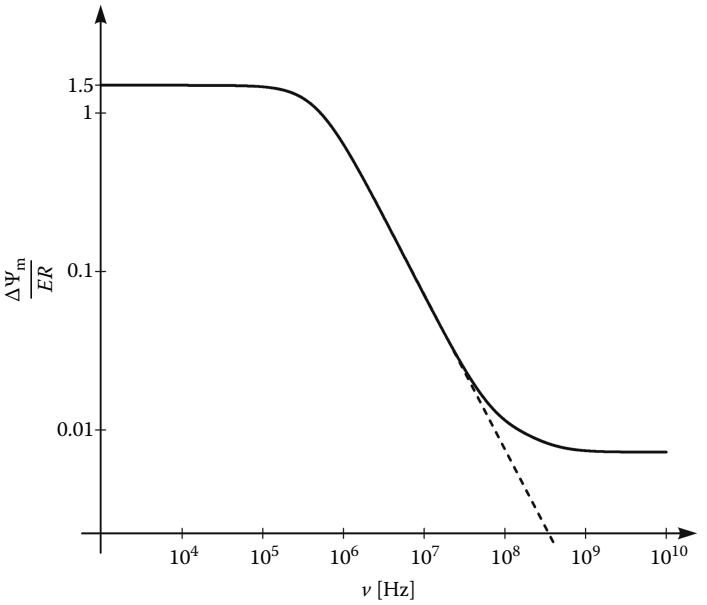

FIGURE 3.6 The amplitude of normalized $\Delta\Psi_m$ as a function of the frequency of the AC field. The dashed curve shows the first-order Schwan's equation, and the solid one the second-order Schwan's equation. Note that both axes are logarithmic.

3.3 Numerical Computation

Realistic cells can deviate considerably from regular shapes considered in Section 3.2. Moreover, in actual situations, cells are rarely isolated, and when sufficiently close to each other, the mutual distortion of the field they cause cannot be neglected. Often, the cells are even in direct contact, forming two-dimensional (monolayers attached to the bottom of a dish) or three-dimensional structures (tissues), and they can even be interconnected by structures such as gap junctions. None of these cases allows for analytical derivation of the induced transmembrane voltage ($\Delta\Psi_m$), while employing analytical solutions for spherical, spheroidal, or cylindrical cells as approximations can lead to rather large errors. In practice, there are two approaches for obtaining accurate estimates of $\Delta\Psi_m$ on irregularly shaped cells: numerical computation and experimental determination. Here, we focus on the numerical methods, while the experimental approach will be the subject of Section 3.4.

3.3.1 Computational Methods

Numerical computation of $\Delta\Psi_m$ is generally performed in several steps. First, the continuous geometry of the model and/or the differential equations describing the electric or electromagnetic field are transformed into their discrete counterparts. Next, these equations are solved either directly or iteratively until adequate convergence is reached. Finally, the electric potential on both sides of the membrane is extracted from the computed data, and $\Delta\Psi_m$ is computed as their difference. Elementary methods, such as solving a linear system of equations, are mostly inadequate for this purpose, while advanced methods, such as the finite difference method and particularly the finite element method, are well suited for this task.

3.3.1.1 Finite Difference Method

The finite difference method is a method for solving differential and integral equations, or systems of such equations. In this method, the continuous geometry of the model is replaced by a grid, which is restricted in the basic form of the method to rectangular shapes and simple alterations thereof. At each grid point, the differential terms of the equation are replaced by the difference terms, and the obtained difference equations are then solved to yield the electric potential in the points of the grid. If this method is used to solve time-dependent partial differential equations (so that time also proceeds in discrete steps), the method is termed the finite-difference time-domain method. The attractive feature of this method is its straightforward implementation, but due to the rectangular mesh it is generally inaccurate with complicated object shapes, and particularly close to the curved boundaries.

3.3.1.2 Finite Element Method

The finite element method is another method for finding approximate solutions of differential and integral equations. The method is based on discretization of the geometry (meshing) into subregions, which are referred to as the finite elements (Reddy 2005). These elements can be of different shapes and sizes, which allow to model intricately shaped objects and to focus on the regions of interest (by making the mesh locally more dense). Similar to the finite difference method, the finite element method can also be extended to time-dependent problems. However, unlike with finite differences, the solution obtained for each finite element is a function varying smoothly between the nodes of the element and preserving the continuity also between the elements. The main advantage of the finite element method is its ability to handle complicated geometries and boundaries with relative ease, and while some attempts were made to model irregularly shaped cells or clusters of such cells with finite differences, these were confined to a 2-D space (Gowrishankar and Weaver 2003, Esser et al. 2007, Joshi et al. 2008). In contrast, the finite element approach can handle realistic 3-D shapes quite easily (Miller and Henriquez 1988, Pucihar et al. 2006, 2009a), and in the next section we illustrate this in more detail.

3.3.2 Irregularly Shaped Cells

Before discretization, a realistic model of the cell under consideration must be constructed and stored in the computer. While this process is straightforward for cells of simple geometric shapes (e.g., cells in suspension can be modeled as spheres), it becomes problematic when irregularly shaped cells are modeled (an extreme example of this is a nerve cell). During discretization, an even more compelling problem occurs, namely, the meshing of the cell membrane, which is over 1000-fold thinner than the dimensions of a typical cell. Even the modern adaptive-size meshing methods generally fail when such disproportions are involved. Another condition related to the membrane meshing that is difficult to meet is the uniform membrane thickness. Once all these difficulties are overcome, the final step is the computation of the electric potential and hence of the induced transmembrane voltage.

3.3.2.1 Constructing a 3-D Model of the Cell

The simplest approach in modeling an irregularly shaped cell is to compose it from several simple geometrical objects (e.g., hemispheres, circular or elliptic cylinders) (Fear and Stuchly 1998, Buitenweg et al. 2003, Valič et al. 2003, Huang et al. 2004). However, typical cells growing in a dish or in a tissue have markedly irregular shapes, and this approach can only yield a rough approximation of the actual situation.

A more realistic three-dimensional model of an irregularly shaped cell can be constructed from a sequence of cross sections of the cell under consideration, as sketched in Figure 3.7. The cross sections are obtained by staining the cell with a membrane marker and acquiring images in different focal

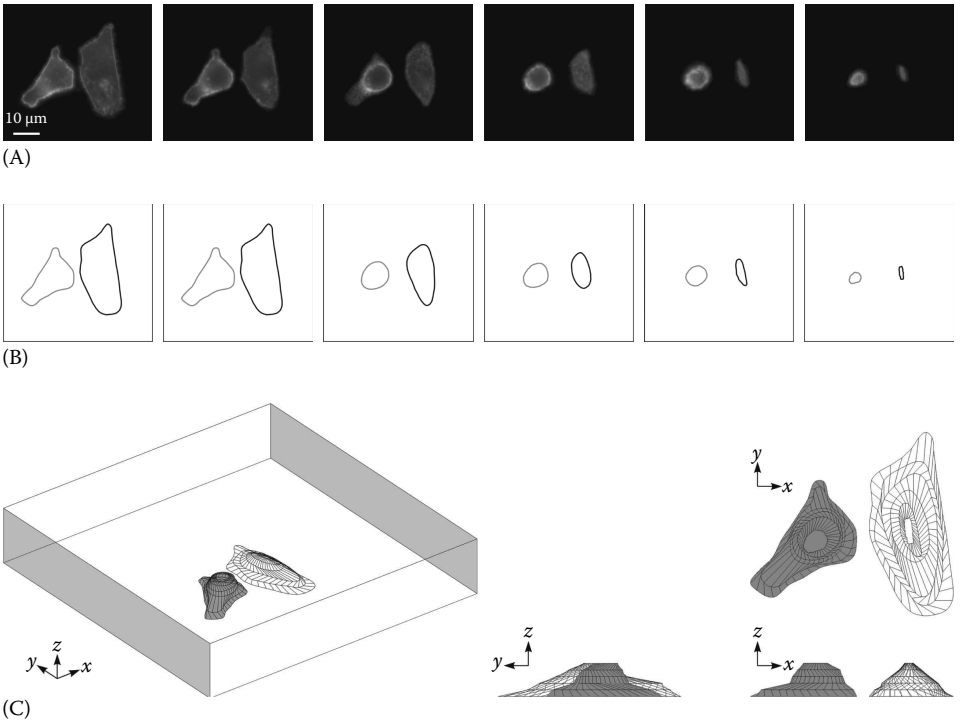

FIGURE 3.7 Construction of a 3-D model of two irregularly shaped CHO cells. (A) Fluorescence cross-section images of the cells stained with di-8-ANEPPS, acquired from the bottom to the top of the cells in 1 μm steps. (B) The contours. (C) The 3-D model in COMSOL Multiphysics 3.4. The interior of the rectangular block represents the extracellular medium, the gray-shaded faces are the electrodes, and the other four faces are insulating. (Adapted from Pucihar G. et al., *Ann. Biomed. Eng.*, 34, 642, 2006.)

planes. In these images, the contours of the cell are then detected, transformed into solid planes, combined into a 3-D object, and imported into the workspace of a finite element software, such as COMSOL Multiphysics (COMSOL Inc., Burlington, MA).

3.3.2.2 Modeling the Cell Membrane

The normal component of the current density in the membrane, J, is given by

$$J(t) = \frac{\sigma_m\left(\Psi_i(t) - \Psi_e(t)\right)}{d} + \frac{\varepsilon_m}{d}\frac{\partial\left(\Psi_i(t) - \Psi_e(t)\right)}{\partial t} \tag{3.23}$$

with σ_m, ε_m, d, Ψ_i, and Ψ_e having the same meaning as in Equations 3.13, 3.15, and 3.19. The first term on the right-hand side represents the conductive component, and the second term the capacitive component of the electric current flowing through the membrane.

When constructing a finite element model of the cell, direct incorporation of a realistic cell membrane (i.e., a very thin layer of uniform thickness enclosing the cell) would require the model to consist locally of an extremely large number of finite elements. Even with the modern adaptive-size mesh generation algorithms, this is often prohibitively time consuming and demanding on computer memory. However, unless the spatial distribution of the electric potential inside the membrane is of interest, this can be avoided. Namely, as far as the electric potentials in the cytoplasm and the cell exterior are concerned, the effect of the membrane with thickness d, electric conductivity σ_m, and dielectric permittivity ε_m is equivalent to the effect of an interface with thickness 0 (i.e., a mathematical surface) separating these two regions and characterized by surface electric conductivity $\kappa_m = \sigma_m/d$, and surface dielectric permittivity $\beta_m = \varepsilon_m/d$. Thus, we can rewrite Equation 3.23 as

$$J(t) = \kappa_m\left(\Psi_i(t) - \Psi_e(t)\right) + \beta_m\frac{\partial\left(\Psi_i(t) - \Psi_e(t)\right)}{\partial t} \tag{3.24}$$

Despite the membrane as such being absent from the model, the drop of electric potential at such an interface is equivalent to the $\Delta\Psi_m$ induced on the membrane characterized by corresponding values of d, σ_m, and ε_m. In models constructed in this way, the mesh of finite elements is generated without difficulty, as disproportionally small elements corresponding to the membrane interior are avoided (Pucihar et al. 2006, 2009a). By assuming that κ_m is a function of $\Delta\Psi_m$, this approach can be extended further, e.g., to simulate the course of electroporation (Pucihar et al. 2009a).

3.3.2.3 Computation of $\Delta\Psi_m$

In COMSOL Multiphysics, the electric potential Ψ is computed numerically by solving the discretized form of Equation 3.1, where σ and ε are the electric conductivity and dielectric permittivity of each region under consideration. In general, this gives Ψ as a function of both space and time, and thus describes both the transient and the steady state. The induced transmembrane voltage, $\Delta\Psi_m(t)$, is then calculated as the difference between electric potentials on both sides of the membrane:

$$\Delta\Psi_m = \Psi_i(t) - \Psi_e(t) \tag{3.25}$$

While the results obtained in this manner are quite accurate, they are only applicable to the particular cell shape for which they were computed. Figure 3.8 displays the steady-state $\Delta\Psi_m(p)$ computed for the two irregularly shaped cells shown in Figure 3.7.

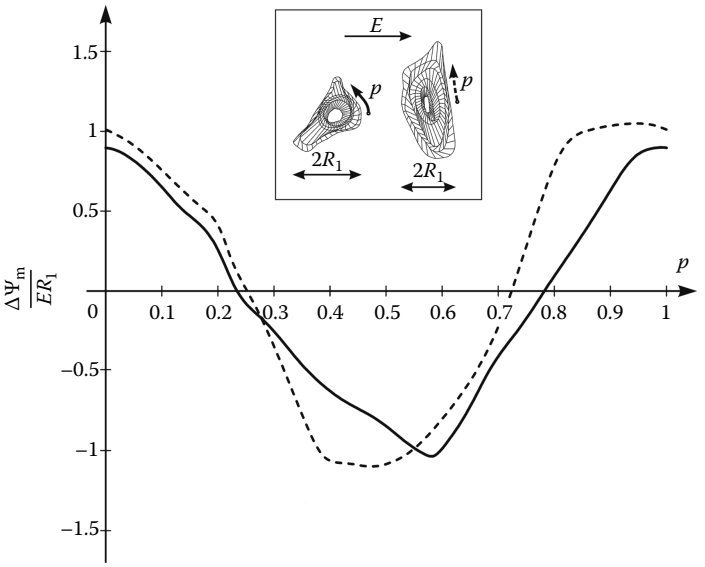

FIGURE 3.8 Normalized steady-state $\Delta\Psi_m(p)$ for two irregularly shaped cells from Figure 3.7. (Adapted from Pucihar G. et al., *Ann. Biomed. Eng.*, 34, 642, 2006.)

3.3.3 Cells in Dense Suspensions and Tissues

In dilute cell suspensions, the distance between the cells is much larger than the cell sizes themselves, and the local field outside each cell is practically unaffected by the presence of other cells. Thus, for cells representing less than 1% of the suspension volume (for a spherical cell with a radius of 10 µm, this means up to 2 million cells/mL), the deviation of the induced transmembrane voltage from the prediction given by Schwan's equation (3.18) is negligible. However, for larger volume fractions occupied by the cells, the distortion of the local field around each cell by the adjacent cells becomes more pronounced, and the deviation from Schwan's equation is also larger (Figure 3.9). For suspensions with cell volume fractions over 10%, as well as for cells in clusters and lattices, a reliable determination of $\Delta\Psi_m$ requires numerical computation (Susil et al. 1998, Pavlin et al. 2002, Pucihar et al. 2007). Regardless of the volume fraction they occupy, as long as the cells are suspended, they float freely, and their arrangement is rather uniform. Asymptotically, this would correspond to a face-centered lattice, and this lattice is also the most appropriate for the analysis of the transmembrane voltage induced on cells in suspension.

For even larger volume fractions, the electrical properties of the suspension start to resemble that of a tissue, but only to a certain extent. The arrangement of cells in tissues does not necessarily resemble a face-centered lattice, since cells can form specific structures (e.g., layers). In addition, cells in tissues can be directly electrically coupled (e.g., through gap junctions). Numerical modeling and computation of electric fields and currents in tissues is discussed in detail in Chapter 15.

3.4 Experimental Determination

An alternative to the analytical and numerical methods for determining the induced transmembrane voltage ($\Delta\Psi_m$) are the experimental techniques. These include the measurements of $\Delta\Psi_m$ with microelectrodes and with potentiometric fluorescent dyes. Microelectrodes (either conventional or patch clamp) were used in pioneering measurements of the action potential propagation (Ling and Gerard

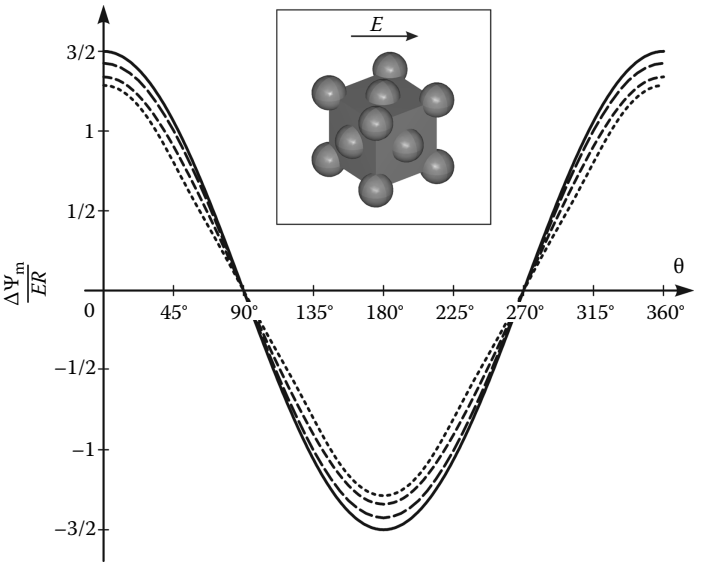

FIGURE 3.9 Normalized steady-state $\Delta\Psi_m(\theta)$ for spherical cells in suspensions of various densities (intercellular distances). Solid: The analytical result for a single cell as given by Equation 3.18. Dashed: numerical results for cells arranged in a face-centered cubic lattice and occupying (with decreasing dash size) 10%, 30%, and 50% of the total suspension volume.

1949, Neher and Sakmann 1976) and were preferred for their simple use and high temporal resolution. However, the invasive nature of measurements and low spatial resolution are considerable shortcomings of this approach. Moreover, the physical presence of the electrodes during the measurement affects the distribution of the electric field around them, and thus also the value of $\Delta\Psi_m$. In contrast, measurement by means of potentiometric dyes is noninvasive, offers higher spatial resolution, does not distort the field and thus $\Delta\Psi_m$. Moreover, it can be performed simultaneously on a number of cells. For these reasons, during the last decades, the potentiometric dyes have become the preferred tool in experimental studies and measurements of $\Delta\Psi_m$.

3.4.1 Potentiometric Dyes

Based on their response mechanism, potentiometric dyes are divided into two classes (Invitrogen Corp. 2009): (1) slow potentiometric dyes that are translocated across the membrane by an electrophoretic mechanism, which is accompanied by a fluorescence change and (2) fast potentiometric dyes that incorporate into the membrane, with their electronic structure and consequently their fluorescence properties dependent on transmembrane voltage.

Electric pulses used in electrophysiological and electroporation-based applications usually have durations in the range of microseconds to milliseconds. In order to measure $\Delta\Psi_m$ induced by such pulses, fast potentiometric dyes have to be used. These dyes respond to changes in $\Delta\Psi_m$ within microseconds or less, which makes them suitable even for measurements of the transient effects. Slow dyes, on the other hand, need several seconds to respond to a change of $\Delta\Psi_m$.

One of the fast potentiometric dyes widely used for measuring $\Delta\Psi_m$ is di-8-ANEPPS (di-8-butylamino-naphthyl-ethylene-pyridinium-propyl-sulfonate), developed by Leslie Loew and colleagues at the University of Connecticut (Fluhler et al. 1985, Gross et al. 1986, Loew 1992). This dye is nonfluorescent in water, but becomes strongly fluorescent when incorporated into the lipid bilayer of the cell membrane, thereby making the membrane highly visible. This enables the construction of numerical

models of cells from microscopic fluorescence images, as described in Section 3.3, and thereby provides a possibility to compute $\Delta\Psi_m$ on the same cells on which an experiment was carried out.

The fluorescence intensity of di-8-ANEPPS varies proportionally to the change of $\Delta\Psi_m$; the response of the dye is linear for voltages ranging from −280 to +250 mV (Lojewska et al. 1989, Cheng et al. 1999). Relatively small changes in fluorescence of the dye, uneven membrane staining, and dye internalization make di-8-ANEPPS less suitable for absolute measurements of membrane voltage, such as the resting membrane voltage, although such efforts were also reported (Zhang et al. 1998). It is, however, well suited for measuring larger changes in membrane voltage, such as the onset of induced transmembrane voltage in nonexcitable cells exposed to external electric fields (Gross et al. 1986, Montana et al. 1989), or action potentials in excitable cells (Bedlack et al. 1994, Cheng et al. 1999). di-8-ANEPPS also allows for determination of $\Delta\Psi_m$ by ratiometric measurements of fluorescence excitation (Montana et al. 1989, Hayashi et al. 1996) or emission (Knisley et al. 2000), which increases the sensitivity of the response.

3.4.2 Image Acquisition and Data Processing

Since the sensitivity of fast potentiometric dyes to the changes of $\Delta\Psi_m$ is low (typically, a change of $\Delta\Psi_m$ by 100 mV results in the change of fluorescence intensity by 2%–12%), the fluorescence changes are hardly discernible by the naked eye and become apparent only after image processing and analysis.

This procedure is performed in several steps (Pucihar et al. 2009b). The first step is acquiring a pair of images: a control image (immediately before the exposure to the electric field) and the pulse image (during the exposure). To get a more reliable measurement, a sequence of pulses can be applied, with both the control and the pulse image acquired for each pulse. The background fluorescence is then subtracted from both images. For the cell under investigation, the region of interest corresponding to the membrane is determined, and the fluorescence intensities along this region in the control and pulse image are measured. For each pulse, the control data are subtracted from the pulse data, and the result divided by the control data to obtain the relative fluorescence changes. If a sequence of pulses is applied, the values of relative fluorescence changes determined for each pulse can be averaged. The relative fluorescence changes are then transformed into values of $\Delta\Psi_m$ using a calibration curve. A rough estimation of this curve can be obtained from the literature, but for higher accuracy, it has to be measured for each particular setup, as shown in Figure 3.10. Calibration is performed with either (1) potassium

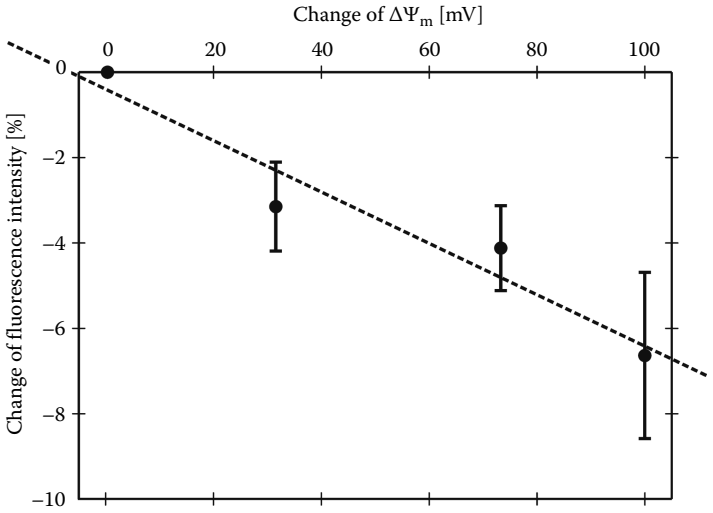

FIGURE 3.10 The calibration curve for measurements of $\Delta\Psi_m$ using di-8-ANEPPS.

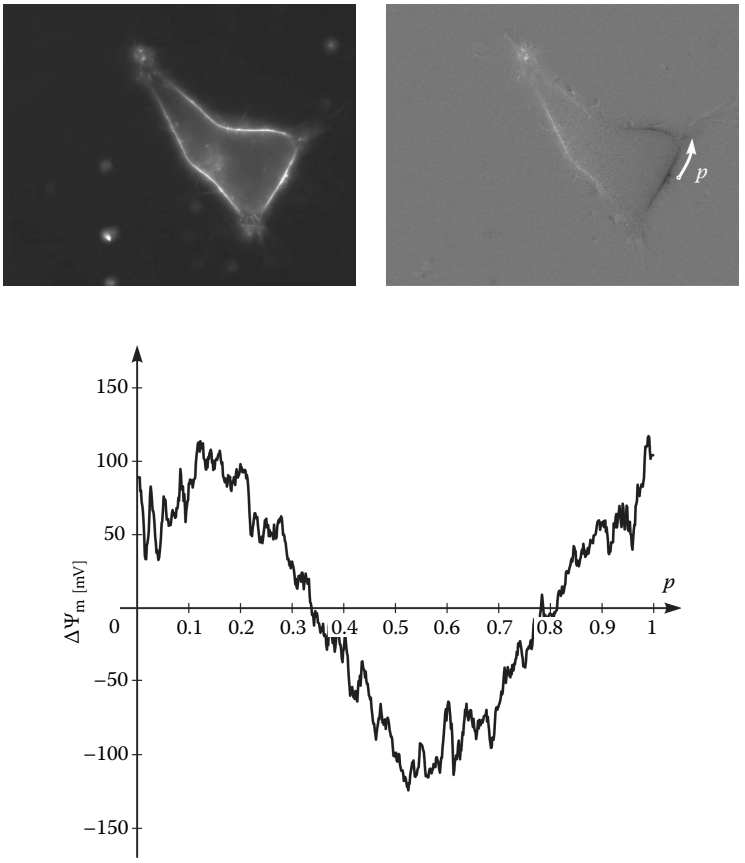

FIGURE 3.11 Determination of steady-state $\Delta\Psi_m$ using di-8-ANEPPS. Top left: Raw fluorescence image of a cell stained with di-8-ANEPPS. Top right: Processed image. Bottom: $\Delta\Psi_m(p)$ determined from the image using the calibration curve shown in Figure 3.10.

ionophore valinomycin and a set of different potassium concentrations in external medium (Montana et al. 1989, Pucihar et al. 2006), or (2) patch clamp in voltage clamp mode (Zhang et al. 1998; Pakhomov and Pakhomova 2010). Finally, the voltage is plotted as a function of the relative arc length. To remove some of the noise inherent to potentiometric measurements, the curve can be smoothed using a suitable filter (e.g., the moving average). Figure 3.11 shows a cell stained with di-8-ANEPPS, the processed image reflecting $\Delta\Psi_m$, and the plot of $\Delta\Psi_m$ along the cell membrane.

Acknowledgment

This work was supported by the Slovenian Research Agency (Programme P2-0249 and Project Z2-9229).

References

Bedlack RS, Wei M, Fox SH, Gross E, Loew LM. 1994. Distinct electric potentials in soma and neurite membranes. *Neuron* 13: 1187–1193.

Beebe SJ, Fox PM, Rec LJ, Willis EL, Schoenbach KH. 2003. Nanosecond, high-intensity pulsed electric fields induce apoptosis in human cells. *FASEB J* 17: 1493–1495.

Buitenweg JR, Rutten WL, Marani E. 2003. Geometry-based finite-element modeling of the electrical contact between a cultured neuron and a microelectrode. *IEEE Trans Biomed Eng* 50: 501–509.

Burnett P, Robertson JK, Palmer JM, Ryan RR, Dubin AE, Zivin RA. 2003. Fluorescence imaging of electrically stimulated cells. *J Biomol Screen* 8: 660–667.

Cheng DK, Tung L, Sobie EA. 1999. Nonuniform responses of transmembrane potential during electric field stimulation of single cardiac cells. *Am J Physiol* 277: H351–H362.

Esser AT, Smith KC, Gowrishankar TR, Weaver JC. 2007. Towards solid tumor treatment by irreversible electroporation: Intrinsic redistribution of fields and currents in tissue. *Technol Cancer Res Treat* 6: 261–273.

Fear EC, Stuchly MA. 1998. Modeling assemblies of biological cells exposed to electric fields. *IEEE Trans Biomed Eng* 45: 1259–1271.

Fluhler E, Burnham VG, Loew LM. 1985. Spectra, membrane binding, and potentiometric responses of new charge shift probes. *Biochemistry* 24: 5749–5755.

Gimsa J, Wachner D. 2001. Analytical description of the transmembrane voltage induced on arbitrarily oriented ellipsoidal and cylindrical cells. *Biophys J* 81: 1888–1896.

Gowrishankar TR, Weaver JC. 2003. An approach to electrical modeling of single and multiple cells. *Proc Natl Acad Sci U S A* 100: 3203–3208.

Gross D, Loew LM, Webb W. 1986. Optical imaging of cell membrane potential changes induced by applied electric fields. *Biophys J* 50: 339–348.

Grosse C, Schwan HP. 1992. Cellular membrane potentials induced by alternating fields. *Biophys J* 63: 1632–1642.

Hayashi Y, Zviman MM, Brand JG, Teeter JH, Restrepo D. 1996. Measurement of membrane potential and $[Ca^{2+}]_{(i)}$ in cell ensembles: Application to the study of glutamate taste in mice. *Biophys J* 71: 1057–1070.

Huang X, Nguyen D, Greve DW, Domach MM. 2004. Simulation of microelectrode impedance changes due to cell growth. *IEEE Sensors J* 4: 576–583.

Huang CJ, Harootunian A, Maher MP, Quan C, Raj CD, McCormack K, Numann R, Negulescu PA, Gonzalez JE. 2006. Characterization of voltage-gated sodium-channel blockers by electrical stimulation and fluorescence detection of membrane potential. *Nat Biotechnol* 24: 439–446.

Invitrogen Corp. 2009. *Molecular Probes—The Handbook*. Carlsbad, CA: Invitrogen Corp. (available electronically at http://www.invitrogen.com/site/us/en/home/References/Molecular-Probes-The-Handbook.html).

Joshi RP, Mishra A, Schoenbach KH. 2008. Model assessment of cell membrane breakdown in clusters and tissues under high-intensity electric pulsing. *IEEE Trans Plasma Sci* 36: 1680–1688.

Knisley SB, Justice RK, Kong W, Johnson PL. 2000. Ratiometry of transmembrane voltage-sensitive fluorescent dye emission in hearts. *Am J Physiol Heart Circ Physiol* 279: H1421–H1433.

Kotnik T, Miklavčič D. 2000a. Second-order model of membrane electric field induced by alternating external electric fields. *IEEE Trans Biomed Eng* 47: 1074–1081.

Kotnik T, Miklavčič D. 2000b. Analytical description of transmembrane voltage induced by electric fields on spheroidal cells. *Biophys J* 79: 670–679.

Kotnik T, Miklavčič D. 2006. Theoretical evaluation of voltage inducement on internal membranes of biological cells exposed to electric fields. *Biophys J* 90: 480–491.

Kotnik T, Bobanović F, Miklavčič D. 1997. Sensitivity of transmembrane voltage induced by applied electric fields—A theoretical analysis. *Bioelectrochem Bioenerg* 43: 285–291.

Kotnik T, Miklavčič D, Slivnik T. 1998. Time course of transmembrane voltage induced by time-varying electric fields—A method for theoretical analysis and its application. *Bioelectrochem Bioenerg* 45: 3–16.

Ling G, Gerard RW. 1949. The normal membrane potential of frog sartorius fibers. *J Cell Comp Physiol* 34: 383–396.

Loew LM. 1992. Voltage sensitive dyes: Measurement of membrane potentials induced by DC and AC electric fields. *Bioelectromagnetics* Suppl. 1: 179–189.

Lojewska Z, Farkas DL, Ehrenberg B, Loew LM. 1989. Analysis of the effect of medium and membrane conductance on the amplitude and kinetics of membrane potentials induced by externally applied electric fields. *Biophys J* 56: 121–128.

Miller CE, Henriquez CS. 1988. Three-dimensional finite element solution for biopotentials: Erythrocyte in an applied field. *IEEE Trans Biomed Eng* 35: 712–718.

Montana V, Farkas DL, Loew LM. 1989. Dual-wavelength ratiometric fluorescence measurements of membrane-potential. *Biochemistry* 28: 4536–4539.

Neher E, Sakmann B. 1976. Single-channel currents recorded from membrane of denervated frog muscle fibres. *Nature* 260: 779–802.

Neumann E, Kakorin S, Toensing K. 1999. Fundamentals of electroporative delivery of drugs and genes. *Bioelectrochem Bioenerg* 48: 3–16.

Pakhomov AG, Pakhomova ON. 2010. Nanopores: A distinct transmembrane passageway in electroporated cells. In: *Advanced Electroporation Techniques in Biology and Medicine*. Boca Raton, FL: Taylor & Francis.

Pauly H, Schwan HP. 1959. Über die Impedanz einer Suspension von kugelförmigen Teilchen mit einer Schale. *Z Naturforsch* 14B: 125–131.

Pavlin M, Pavšelj N, Miklavčič D. 2002. Dependence of induced transmembrane potential on cell density, arrangement, and cell position inside a cell system. *IEEE Trans Biomed Eng* 49: 605–612.

Pucihar G, Kotnik T, Valič B, Miklavčič D. 2006. Numerical determination of the transmembrane voltage induced on irregularly shaped cells. *Ann Biomed Eng* 34: 642–652.

Pucihar G, Kotnik T, Teissié J, Miklavčič D. 2007. Electroporation of dense cell suspensions. *Eur Biophys J* 36: 173–185.

Pucihar G, Miklavčič D, Kotnik T. 2009a. A time-dependent numerical model of transmembrane voltage inducement and electroporation of irregularly shaped cells. *IEEE Trans Biomed Eng* 56: 1491–1501.

Pucihar G, Kotnik T, Miklavčič D. 2009b. Measuring the induced membrane voltage with di-8-ANEPPS. *J Vis Exp* 33: 1659 (available as video at http://www.jove.com/index/details.stp?ID=1659).

Reddy JN. 2005. *An Introduction to the Finite Element Method,* 3rd edn. New York: McGraw-Hill.

Schoenbach KH, Beebe SJ, Buescher ES. 2001. Intracellular effect of ultrashort electrical pulses. *Bioelectromagnetics* 22: 440–448.

Sharma V, Tung L. 2004. Ionic currents involved in shock-induced nonlinear changes in transmembrane potential responses of single cardiac cells. *Pflugers Arch* 449: 248–256.

Susil R, Šemrov D, Miklavčič D. 1998. Electric field induced transmembrane potential depends on cell density and organization. *Electro Magnetobiol* 17: 391–399.

Teissié J, Eynard N, Gabriel B, Rols MP. 1999. Electropermeabilization of cell membranes. *Adv Drug Deliv Rev* 35: 3–19.

Tekle E, Oubrahim H, Dzekunov SM, Kolb JM, Schoenbach KH, Chock PB. 2005. Selective field effects on intracellular vacuoles and vesicle membranes with nanosecond electric pulses. *Biophys J* 89: 274–284.

Valič B, Golzio M, Pavlin M, Schatz A, Faurie C, Gabriel B, Teissié J, Rols MP, Miklavčič D. 2003. Effect of electric field induced transmembrane potential on spheroidal cells: Theory and experiment. *Eur Biophys J* 32: 519–528.

Zhang J, Davidson RM, Wei MD, Loew LM. 1998. Membrane electric properties by combined patch clamp and fluorescence ratio imaging in single neurons. *Biophys J* 74: 48–53.